Recycling alginate composites for thermal insulation

Matteo Cibinel [a,*], Giorgia Pugliese [a], Davide Porrelli [b], Lucia Marsich [a], Vanni Lughi [a]

[a] Department of Engineering and Architecture, University of Trieste, Via Valerio 6/1, 34127, Trieste, Italy
[b] Department of Medicine, Surgery and Health Sciences, University of Trieste, Piazza dell'Ospitale 1, 34125, Italy

ARTICLE INFO

Keywords:
Alginate
EDTA
Thermal insulation
Recycling
Chelation
Composite

ABSTRACT

We present a new method for the total functional recycling of alginate-based composite materials made via ionotropic gelation. The original material, an alginate/fiberglass foam with thermal insulation characteristics, was produced following a patented process in which fiberglass waste is embedded into the polyanionic gel matrix, and the resulting compound is then freeze-dried. The functional recycling is carried out by disassembling the ionic matrix – which is initially formed by the interaction between a cation (e.g. calcium) and the negatively charged alginate backbone – with the use of a chelator (Ethylenediaminetetraacetic acid disodium salt) with a high affinity for the cations, thus obtaining a homogeneous solution. An ionotropic gel can then be re-formed upon deactivation of the chelating activity under mild acid conditions. We managed to maintain or improve the thermal, mechanical and acoustic performances of the original material and we successfully tested the possibility of multiple recycling cycles.

1. Introduction

Green chemistry, energy efficiency, sustainability and recyclability are just some of the keywords that describe the environmental awareness currently leading the development of new eco-sustainable materials and technologies to be implemented in the near future society. A drastic cut in energy demand and CO_2 emission is mandatory in order to mitigate the effects of global warming (Masson-Delmotte et al., 2018). It has been estimated that, globally, buildings account for more than 10 % of the total final energy consumption for heating and cooling needs (Ürge-Vorsatz, Cabeza, Serrano, Barreneche, & Petrichenko, 2015). In this scenario, the reduction of energy losses due to the use of inefficient or insufficient thermal insulation systems is crucial, and novel technologies having a low environmental footprint are expected to play a decisive role. Currently, many different classes of insulation materials are commercialized and can be categorized as inorganic, petroleum-derived and natural organic materials. Inorganic thermal insulators, such as mineral wools, together with petroleum-derived polymeric foams (such as expanded polystyrene and polyurethane) are the major players, sharing together more than 90 % of the European market (Pavel & Blagoeva, 2018). Unfortunately, these conventional insulation materials are either obtained from oil-derived chemical substances, or high temperatures are needed to process the raw materials (Asdrubali, D'Alessandro, & Schiavoni, 2015). Moreover, some concerns about health risks linked with the handling and storage of mineral wools are under discussion (Harrison et al., 2015). For these reasons there is a real interest in developing replacement materials (Caniato, Sbaizero, Schmid, & Bettarello, 2015). As far as petroleum-derived materials like polyurethane and expanded polystyrene are concerned, even if some recycling technologies are available (Kemona & Piotrowska, 2020; Thakur et al., 2018), the waste is mainly disposed of at the landfills, or incinerated due to economical or energetic convenience, thus enhancing the demand of non-renewable resources to replace the lost insulation materials (Lassen et al., 2019).

Natural materials are now getting attention thanks to their reduced environmental impact and their low cost: cotton, cork and wood fiber based panels are already commercialized. Moreover, the added value of the negative CO_2 balance (Asdrubali, Schiavoni, & Horoshenkov, 2012) and better biodegradability brace the research interest in plants-derived materials: hemp (Nguyen et al., 2016), kenaf (Ardente, Beccali, Cellura, & Mistretta, 2008; Erkmen, Yavuz, Kavci, & Sari, 2020), rice and wheat husk (Muthuraj, Lacoste, Lacroix, & Bergeret, 2019) are just a few examples of raw materials from which thermal insulation panels can be obtained.

Industrial waste can also be used as recycled feedstock for new thermal insulation panels: glass waste has been used by A. Ayadi and coworkers (Ayadi, Stiti, Boumchedda, Rennai, & Lerari, 2011) whereas Valverde (Valverde, Castilla, Nuñez, Rodriguez-Senín, & De La Mano

* Corresponding author at: Department of Engineering and Architecture, University of Trieste, Via Valerio 6, Trieste, I-34127, Italy.
E-mail address: matteo.cibinel@phd.units.it (M. Cibinel).

Accepted 22 August 2020

Ferreira, 2013) used thermoformed polyester and polyurethane textile industry offcuts. Recycled PET, nylon/spandex fibers, wool, cotton and other materials can be added to the list and a comprehensive review has been published on the topic (Asdrubali et al., 2015). All of the above-mentioned solutions contribute to the reduction of the use of virgin feedstock and the initial disposal of waste in the landfills.

Alginate is a natural copolymer, primarily extracted from brown seaweed, which is capable to form a physical gel upon interaction with divalent (or trivalent) cations. It has numerous applications: in the food industry, as edible thickening agent (Qin, Jiang, Zhao, Zhang, & Wang, 2018), in biology and medicine, as drug delivery system (Zheng et al., 2017), wound dressing and tissue engineering (Lee & Mooney, 2012) mainly due to its biocompatibility, biodegradability and low cost. Recently, alginate has found application in the field of thermal insulation materials: both Mati-Baouche (Mati-Baouche et al., 2014) and M. Palumbo (Palumbo, Navarro, Giraldo, Lesar, & Lacasta, 2015) used sodium alginate (SA) as a natural binder to produce a thermal insulation bio-composite, and similar applications are found in the literature (Lacoste, El Hage, Bergeret, Corn, & Lacroix, 2018; Muthuraj et al., 2019; Palumbo, Lacasta, Navarro, Giraldo, & Lesar, 2017). Another alginate foam was produced by Thierry Vincent and coworkers (Vincent et al., 2018), who were able to produce a lightweight thermal insulation material with air-drying methods. Unfortunately, even in the case of the above-mentioned materials that can offer a greener alternative to conventional solutions, little or no attention has been paid to the end-of-life options, and disposal (or incineration) is currently regarded as the only available choice.

In this work we present a recycling process for a natural-based thermal insulation foam that has been developed in a previous work (Kyaw Oo D'Amore et al., 2017) which shows remarkable sound absorption and thermal insulation properties. The original foam is produced with a patented process (EP Patent 16425023.5, 2016) in which a SA matrix is used to host industrial waste materials to produce a porous solid structure via a ionotropic-gelification step followed by freeze-drying. Since the SA gel is formed via reversible ionic bonds between SA chains and cations, a chelator with a higher affinity toward the cation can be used to interfere with these bonds, leading to the decomposition of the gel. We specifically investigate the role of Ethylenediaminetetraacetic acid disodium salt (EDTA – 2Na) as chelator agent, while sodium hydroxide (NaOH), hydrochloric acid (HCl) and d-glucono-δ-lactone (GDL) solutions have been used to modulate the chelator activity. With the presented recycling method Ionotropically gelled alginate composites can be fully recycled, maintaining their functional characteristics, via a reversible pH driven selective cations chelation process.

2. Materials

Alginate sodium salt (MW = 200–250 KDa; M/G ratio = 1.44; shear viscosity =0.99 Pa s at 1.4 w/v, 25 °C, 7.5 pH and 1 s-1) and hydrochloric acid (37 % solution) were purchased from Carlo Erba. D-glucono-δ-lactone (GDL), CaCO3 and ethylenediaminetetraacetic acid disodium salt (2Na-EDTA) were purchased from Sigma Aldrich. Sodium Hydroxide was purchased from NORMAPUR® analytical reagent. Milli-q water used to prepare all aqueous solutions was purified with a Direct-Q 5 UV Millipore® system. The fiber-glass powder waste derived from final grinding of fiber-glass products.

3. Methods

3.1. Production of the original alginate foam (oAF)

The original alginate foam (oAF) to be recycled was produced via the method reported previously (EP Patent 16425023.5, 2016; Kyaw Oo D'Amore et al., 2017). Briefly, SA was dispersed in milli-q water, at a concentration of 1.4 w/v, to obtain a homogeneous viscous solution (V – oAF). Fiber-glass powder and calcium carbonate were then added to the SA solution to obtain a final concentration of 5 % w/v and 15 mM, respectively. To initiate the internal gelation, a GDL solution (60 mM) was finally added before pouring the viscous solution in a rectangular mold.

The dry foam was therefore obtained via freeze-drying: the gel within the mold is frozen at −20 °C and after 12 h lyophilized using a Lio 5 P freeze drier. The samples were extracted from the freeze drier, after 48 h, once a plateau in the readings of the internal pressure gauge was reached. All the concentrations are expressed for a final gel volume of 700 ml which corresponds to a single foam tile (200 mm × 200 mm × 18 mm).

3.2. Recycling of the oAF (rAF)

44 mM of 2Na-EDTA were dissolved in Milli-q water at pH 8 (stabilized with 1 M NaOH solution) to obtain a clear solution. A single foam tile of the oAF material, produced as previously described, was ground and then added to the solution. The pH was stabilized at 7.5 using a 0.1 M NaOH solution. The solution was maintained under vigorous stirring for 1 h at a constant pH level. After one hour, a homogeneous viscous solution was obtained (V – rAF). At this point the alginate and fiber-glass concentration in the water solution was equivalent to the one present in the oAF production process prior to the gelification step.

Four different routes have been tested to re-establish the gel structure:

- rAF – CG: addition of $CaCO_3$ (final concentration of 15 mM) followed by the addition of GDL (180 mM)
- rAF – G: addition of GDL (180 mM) without the use of additional $CaCO_3$.
- rAF – CG – A: addition of $CaCO_3$ (final concentration of 15 mM) followed by the addition of GDL (180 mM) and HCl 6 M (0.5 % v/v) at 75 °C
- rAF – G – A: addition of GDL (180 mM) and HCl 6 M (0.5 % v/v) at 75 °C.

Immediately after the addition of GDL the viscous solution was poured in a rectangular mold prior to gelification. The dried foam was obtained following the previously described freeze-drying procedure. All the concentrations are expressed for a final gel volume of 700 ml. All tested formulations are listed in Supporting information Table S1.

3.3. Recycling of the rAF (2rAF)

A second-recycling test was made by dissolution of the rAF – G composition following the procedure described for the production of rAF samples, without the addition of new EDTA. Briefly, a single foam tile of the rAF – G material was ground and then added to a water solution, and the pH was stabilized at 7.5 using a 1 M NaOH solution. The solution was maintained under vigorous stirring for 1 h at a constant pH level. After one hour, a homogeneous viscous solution was obtained. Following the addition of GDL (180 mM), the viscous solution was poured in a rectangular mold prior to gelification. The dried foam was obtained following the previously described freeze-drying procedure. All the concentrations are expressed for a final gel volume of 700 ml. All tested formulations are listed in Supporting information Table S1.

3.4. Rheological characterization

Rheometry was used to characterize the viscoelastic response of the original and recycled material, in order to highlight the influence of 2Na-EDTA concentration and of the use of additional $CaCO_3$ and HCl in the recycling process. To prevent interferences derived from the dispersed particulate, the rheological characterization was performed on samples that had been prepared as previously described, but without

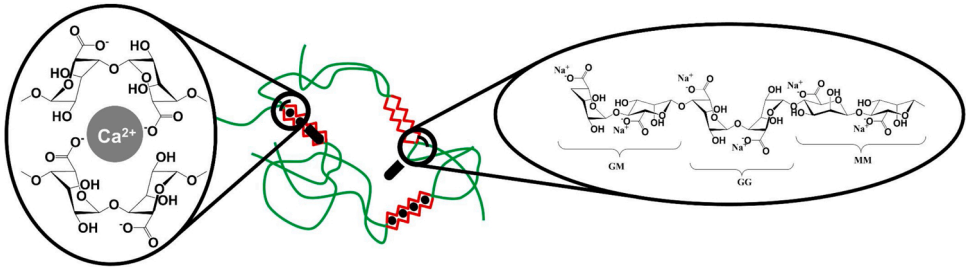

Fig. 1. Alginate gel structure, egg-box model, G = guluronate M = mannuronate.

the addition of fiberglass powder. Different concentration of 2Na-EDTA were tested: 15 mM and 45 mM. Since a single de-protonated EDTA molecule ($EDTA^{4-}$) is capable to chelate a single Ca^{2+} ion; the tested concentration corresponded respectively to one and three equivalents of Ca^{2+} present in the original sample (15 mM).

Steady-state shear viscosity (flow curves) was used to characterize the homogeneous solution obtained after the dissolution of the dried foam; 2 ml of solution were sampled to this purpose. A clean sodium alginate solution at the same concentration and pH (7.5) of the previous has been used as reference. The Cross model was used to fit the flow curves (Cross, 1969) (Eq. (1)):

$$\eta = \eta_\infty + \frac{\eta_0 - \eta_\infty}{1 + (\tau \cdot s)^m} \quad (1)$$

where $\eta$is the viscosity at the shear rate s, η_0 and η_∞ are the extrapolated viscosity at zero and infinite shear rate, respectively. τ is the shear rate at which the viscosity assumes the mean value. m is the exponential fitting parameter, which is inversely proportional to the polydispersity index (PI) of the polymer.

The mechanical behavior of the re-formed gels (i.e. the mechanical spectrum) was determined by performing a dynamic frequency sweep test (FS) within the linear stress regime (2 Pa) previously identified with a short stress sweep test (f =1 Hz; stress range 2−5 Pa; maximum deformation <0.02 %). The viscous (G'') and the elastic (G') components of the mechanical response were then calculated for each sample. A clean alginate sodium alginate gel has been used as reference.

All the rheological tests were performed at 25 °C using the controlled stress rheometer Haake Mars III equipped with Peltier temperature control system and using the cone–plate geometry (flow curves) and a crosshatched plate–plate geometry (frequency sweep and stress sweep).

All the references and tested samples have been prepared with a final gel volume of 100 cm^3 following the previously described procedures. All tested formulations are listed in Supporting information Table S2; the flow curves have been obtained prior to the addition of $CaCO_3$ and GDL.

3.5. Thermal characterization

Specific heat and thermal conductivity have been measured using a NETZSCH HFM 446 Lambda Series. The typical sample size was 200 mm × 200 mm × 18 mm. To ensure a proper contact between the specimen and the sampling area of the instrument, a 2 kPa load was applied. Thermal conductivity was calculated using a steady-state Fourier model at an average temperature of 20 °C and 40 °C. Specific heat values were calculated by integration of the heat flux over time at an average sample temperature of 20 °C and 30 °C. The measurements were performed according to ASTM C 518 and ASTM C1784 standards.

3.6. Acoustic characterization

Sound absorption analysis was performed with a Kundt tube with a diameter of 45 mm according to ISO 10534-2:1998 and ISO 11654:1998. Tests were performed on three samples of 18 mm of thickness.

3.7. Compression test

Compression test were performed using a Shimadzu Autograph 2, AG-10TA equipped with a 100 kN load cell with a constant compression speed of 1.3 mm/min. The tested samples had a square shape with an average side length of 50 mm and an average thickness of 18 mm. The

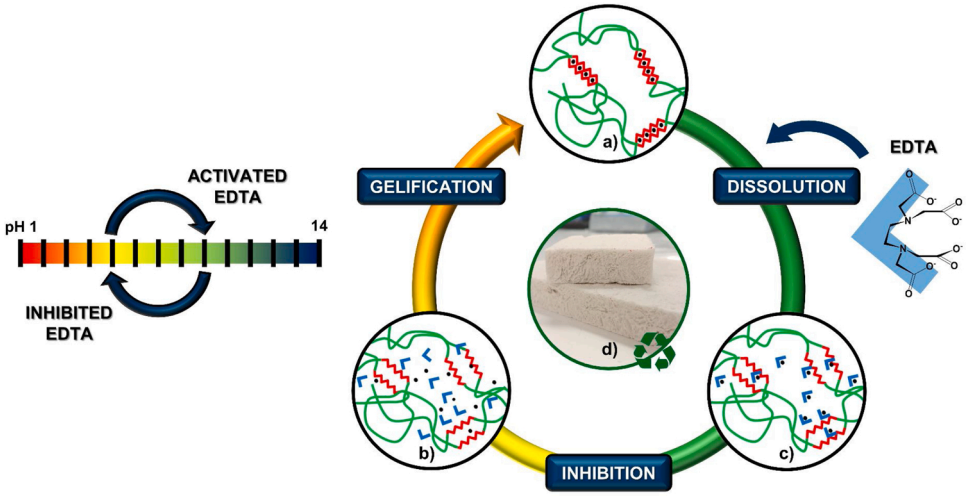

Fig. 2. Representation of the recycling process. The alginate foam (d) is dissolved in activated EDTA solution by subtraction of calcium ions from alginate gel junction zones, obtaining a homogeneous viscous solution (b). Upon inhibition of the chelator, by a pH drift, calcium ions are released (c) and the gel structure is reobtained (a).

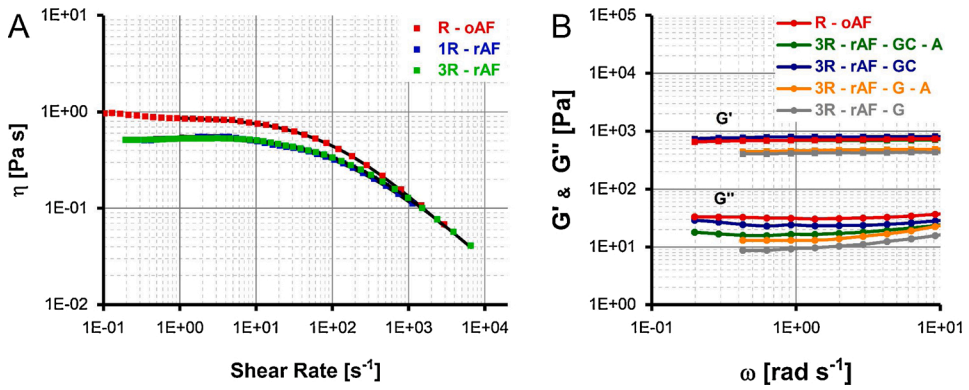

Fig. 3. (A) Rheological Steady state shear viscosity test of original and recycled sample at different EDTA concentration. No glass fibers. Black lines correspond to the Cross-Model fitting. (B) Mechanical spectra of original and recycled alginate gel, no glass fibers added.

compression modulus was determined by the linear deformation regime in the stress-strain curve. Different conditioning procedures were tested to highlight the effect of moisture uptake:

- dry: conditioning for 24 h in a ventilated oven at 45 °C
- 40RH: conditioning in a 44 % RH environment (using a K_2CO_3 saturated solution). The samples, weighted at regular intervals, were tested after a plateau in the percentage weight gain was reached.

Data processing was performed according to ASTM D 1621 standard.

3.8. Scanning electron microscope (SEM) and micro-computed tomography (μCT)

A 10 mm × 10 mm × 10 mm volume was extracted from the center of the sample, and images were collected using a Leica-Stereoscan 430i Scanning Electron Microscope (SEM). X-ray microcomputed tomography (μCT) of samples was obtained by means of a custom-made cone-beam system called TOMOLAB (Elettra, Trieste). m-CT acquisitions were performed with a resolution of 8 μm, beam energy of 40 kV and intensity of 200 μA, and an exposure time 2.5 s. The slices reconstruction process and the correction of artifacts were realized by a commercial software (Cobra Exxim). Pore3D software (Brun et al., 2010) was used for the quantitative analyses. Amira software (Thermo Fisher Scientific, Waltham, USA) was used for the 3D rendering.

4. Results and discussion

4.1. Recycling process

Alginate is an anionic block copolymer composed by (1-4)-linked β-D-Mannuronate (M) and α-L-guluronate residues (G) which is capable to form a reversible physical gel through chelation, from GG blocks, of divalent or trivalent cations (e.g Ca^{2+}, Cu^{2+}, Fe^{3+}) represented by the egg-box model (Fig. 1). This ion-induced gelation is referred to as ionotropic gelation (Agulhon, Robitzer, David, & Quignard, 2012; Ivanova, Bazaka, & Crawford, 2014). To avoid instantaneous and inhomogeneous gelification, following the introduction of cations, a controlled internal gelation approach was used with $CaCO_3$ and GDL: GDL slowly hydrolyze in water forming D-guluronic acid, which, upon acidification of the solution, promotes the release of Ca^{2+} by decomposition of the previously dispersed $CaCO_3$. Once the ionic gel is formed, it can withstand temperatures up to 100 °C (Sergeeva, Vikulina, & Volodkin, 2019).

The recycling process herein described, and depicted in Fig. 2, exploits the reversible ionic interactions that build up the alginate matrix of the oAF samples. Simple grinding and stirring do not lead to the dissolution of the oAF since the calcium alginate gel is stable in water. A chelator, however, capable to interfere with the ionic bonds between the alginate chain and calcium, can subtract the crosslinking-cations, leading to the dissolution of the matrix. The alginate foam can be reobtained by inhibition of the chelator (in mild acid condition) which release the cations that are then available again to crosslink the alginate.

Table 1
Cross model fitting parameters results. Mean absolute deviation in parentheses.

	τ	m	η_0	η_∞
R – oAF	0.010 (0.001)	0.750 (0.009)	1.000 (0.075)	0.003 (0.004)
1R – rAF	0.007 (0.001)	0.724 (0.019)	0.579 (0.063)	0.003 (0.002)
3R – rAF	0.006 (0.001)	0.736 (0.013)	0.601 (0.044)	0.002 (0.002)

During the first part of the process, the condition for the dissolution of the matrix is that the conditional association constant of the chelator, referred to the cation ($K'^{2+}_{EDTA/Ca}$), is larger than the one of the alginate ($K'^{2+}_{Alg/Ca}$). Since only the deprotonated forms, $EDTA^{4-}$ and guluronate residue (G), are capable of binding the cation, the association values change with the pH of the solution due to the change of the fraction of deprotonated species ($\alpha_{EDTA^{4-}}$, α_G):

$$K'_{EDTA-Ca^{2+}} = \alpha_{EDTA^{4-}} \cdot K_{EDTA^{4-}/Ca^{2+}} \quad (2)$$

$$K'_{Alg/Ca^{2+}} = \alpha_G \cdot K_{G/Ca^{2+}} \quad (3)$$

In the first part of the process (i.e. dissolution) the pH of the solution was stabilized at pH = 7.5. At this point the calculated conditional association constant for alginate and EDTA calcium complexes (Table S3 in Supporting information) are 3.99 and 7.88 (Log K values), respectively, achieving the condition for the dissolution of the matrix. Maintaining the pH between 7 and 8 is fundamental to prevent deactivation (via protonation at lower pH level) of the EDTA and the basic degradation of the alginate polymer (Guarino, Caputo, Altobelli, & Ambrosio, 2015; Haug, Larsen, Smidsröd, Munch-Petersen, & Munch-Petersen, 1963). After the sequestration of the calcium ion, a homogeneous and clear solution of alginate was obtained and no residues of the original material were observed. (The treated oAF sample containing fiber-glass powder resulted opaque but still homogeneous).

Steady state-shear viscosity (Fig. 3) has been used to evaluate signs of possible chain degradation, due to the addition of NaOH solution during the process. Both the original and the recycled alginate solution shown a shear thinning behavior, typical of polymeric solutions. The reduction of the zero-shear viscosity (η_0) of the recycled samples is attributed to the presence of the EDTA since an analogous behavior was evident in a control experiment where EDTA was added to a clean alginate solution.

The values and the dispersion of the exponential parameter m in the cross model equation (Eq. (1)), obtained from the data for the original and for the recycled samples (Table 1), are in line with those reported in the literature (Roopa & Bhattacharya, 2009).

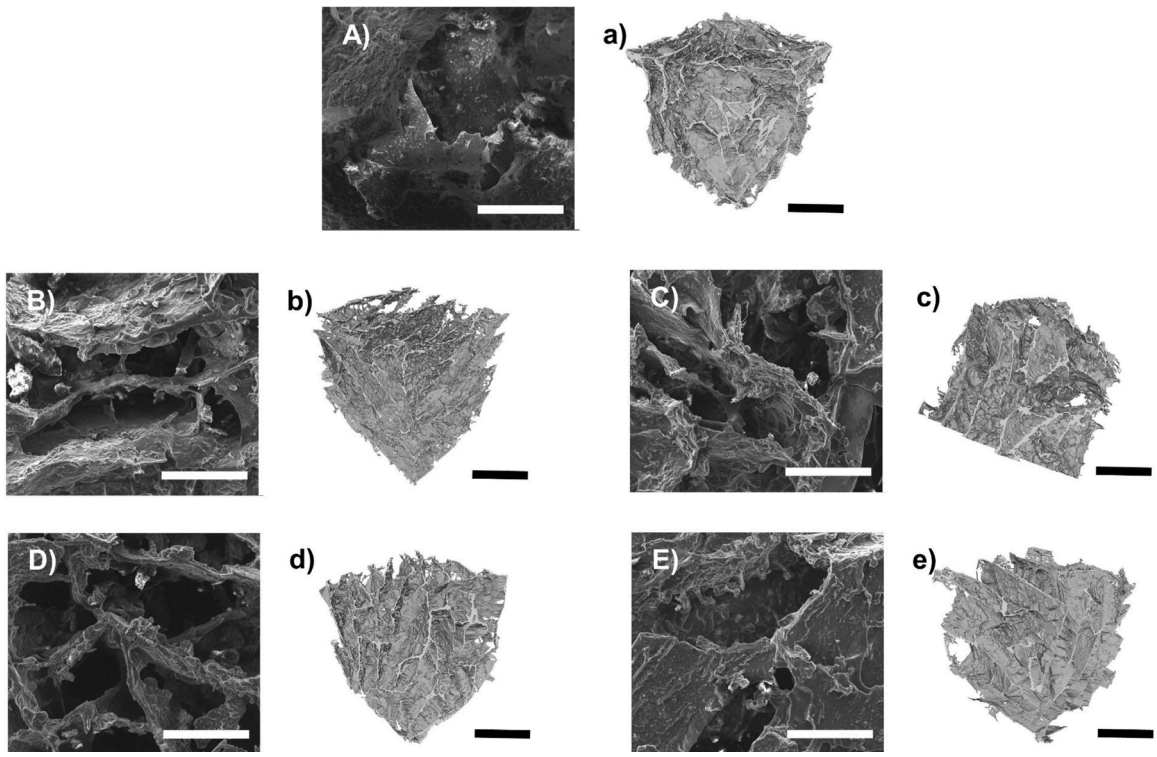

Fig. 4. SEM and μCT images of: (A) (a) oAF; (B) (b) rAF – GC – A ; (C) (c) rAF – GC ; (D) (d) rAF – G – A ; (E) (e) rAF – G; SEM scale bar equal to 500 μm, μCT scale bar equal to 2 mm.

The variations on the value of m, due to uncertainty on the measure, is such that the observed variation cannot be considered meaningful and no sign of polymer degradation can be deduced. In case of degradation, a sharp reduction of the exponential value would be expected since, for linear non-blended polymers, *m* is inversely proportional to the PI of the polymer (i.e. the ratio between the weight averaged molecular weight and the numeric averaged molecular weight $\overline{M}_w/\overline{M}_n$). No differences in the use of the two different EDTA concentrations (15 mM e 45 mM) was detected from the steady-state shear rheology test, therefore only the higher EDTA concentration (45 mM) was used in all rAF samples.

The following step involves the inhibition of the chelator and the subsequent gelification of the matrix. In this phase the pH of the solution is lowered, and the calcium ions bind preferentially to the alginate – i.e. reversing the trend with respect to the dissolution phase. This is due to the different value of the conditional association constant (as presented in Table S3 in Supporting information): Log ($K'^{2+}_{Alg/Ca}$) exceeds the Log ($K'^{2+}_{EDTA/Ca}$) at pH ≈ 4.9. In the literature (Bassett, Håti, Melø, Stokke, & Sikorski, 2016; Yamamoto, Yuguchi, Stokke, Sikorski, & Bassett, 2019), stoichiometric or even lower amounts of GDL, necessary to protonate the four carboxyl group of the EDTA, are used to form a stable ionic alginate gel. The preferential recycling route involves the use of GDL alone (rAF – G). Further addition of $CaCO_3$ after the dissolution phase has been studied in order to increase the concentration of Ca^{2+} available to crosslink the alginate (rAF – GC). With the same purpose the use of HCl was tested to further promote the acidification of the solution and the release of Ca^{2+} from the $(EDTA\text{-}Ca^{2+})^{2-}$ complex (rAF – G – A and rAF – GC – A). The use of GDL is preferred to HCl due to the inhomogeneous gel formation upon contact with a 6 M HCl solution. This is because alginate is also capable to form a weaker gel (i.e. alginic gel) at pH values below 3.5 – 3 due to the protonation of carboxylic groups (Ivanova et al., 2014). To prevent the formation of non-thermally stable alginic gel clusters, in which the HCl remains trapped, it is crucial that the HCl solution (jointly with freshly prepared GDL solution) is added after heating the solution at 75 °C and under vigorous mixing. The assumption that gelification of all rAF samples occurs through ionotropic gelation, avoiding acid gelation, is supported by the fact that the final pH of all rAF gels (before lyophilization) reached a plateau at pH = 4, before the acid gel formation point. The gelification setting time of oAF also changes between formulations: initial setting of oAF takes place in ≈ 30 min whereas for rAF it takes 1–2 h when HCl or additional $CaCO_3$ is used (3R – rAF – G – A, 3R – rAF – GC – A and 3R – rAF – GC). Conversely, 3R – rAF – G samples are characterized by a longer setting time (approximately 3–4 h).

Mechanical Spectra of both oAF and all rAF samples show a frequency-independent behavior of both the storage (G') and the loss (G'') modulus within the linear strain regime (Fig. 3), characteristic of elastic gelled systems. This further supports the fact that the dissolution step did not degrade the polymer, which maintained its gel-forming capabilities.

The G' value in 3R – rAF – G and 3R – rAF – G – A samples is decreased with respect to the storage modulus of oAF and 3R – rAF – GC and 3R – rAF – GC – A, which are similar. This reduction of the magnitude of the storage modulus in the rAF samples is due to the incomplete release of the total amount of chelated Ca^{2+} ions, due to the high association constant of the $(EDTA - Ca^{2+})^{2-}$ complex (Log K = 10.65). A precise control of the concentration of proton-releasing species (e.g. GDL or HCl) into the solution could lead to a better control of the Ca^{2+} exchange between the EDTA and the alginate.

4.2. Morphology

To investigate the morphology SEM images and μCT reconstruction were collected. A well-interconnected millimeter range open porous structure is preserved in all the rAF samples as it can be clearly seen in Fig. 4. Even if a close porous structure is preferred in high performing thermal insulator, it has a detrimental impact on sound insulation performance where pore interconnectivity play a major role (Cao, Fu, Si, Ding, & Yu, 2018). Open cell structure and the presence of a millimeter range porosity also lead to a strong contribution of convection in heat transfer (Fig. 5).

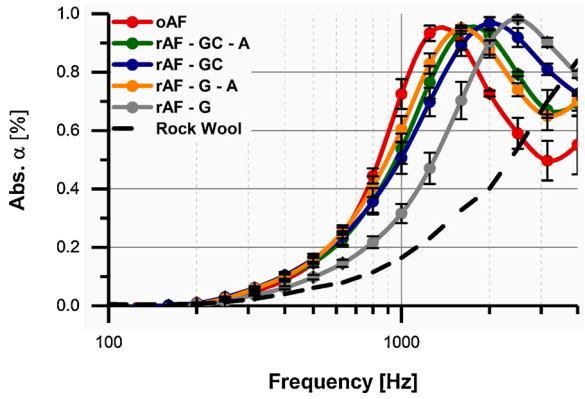

Fig. 5. Averaged sound absorption coefficients of oAF and rAF samples, mean absolute deviation for each datapoint was calculated. Absorption curve of Rockwool has been added as reference from literature (Kyaw Oo D'Amore et al., 2017). Rockwool sample thickness: 10 mm.

4.3. Sound absorption

Sound absorption capability of the rAF is preserved in the recycled samples and is shown to be effective in the human-speech region (500−2000 Hz), as demonstrated in Fig. 6. All rAF samples share an open cell structure with the oAF, which is fundamental for sound absorption: air needs to travel through the material to dissipate energy through viscous, thermal and damping mechanisms (Cao et al., 2018). Preserving an open cell structure in foamy materials represent a compromise to maintain goods sound absorption and thermal insulation performance.

4.4. Thermal properties

Thermal conductivity, density and specific heat capacity are the three main parameters that characterize a thermal insulation material (Table 2 and Fig. 6). A small thermal diffusivity ($a = k / \rho\, c_p$) helps reducing energy consumption in buildings especially in hot climate (Reilly & Kinnane, 2017). Rises in specific heat capacity and of rAF samples are observed upon addition of EDTA and GDL during the recycling process (respectively 12 % wt and 25 % wt). The consequent observed increase in the rAF density leads to a slight increase in thermal conductivity, all although still below the threshold value of 50 mW m^{-1} K^{-1} at 20 °C which is a common indicator for a good thermal insulator material. It is worth noting that rAF – GC – A samples generally possess a lower thermal conductivity with respect to the other rAF samples, despite an average higher density. This could be explained with the different pore size distribution (Fig S1, Supporting information): oAF and rAF – GC – A both possess a lower population of larger pores (in the millimeter range), which mostly contribute to the convection heat transfer.

This also suggests that a better control of the structure of the foam could have a relevant impact on the thermal properties of both oAF and rAF.

The contribution of thermal conductivity, density and specific heat capacity to the overall efficiency of rAF as thermal insulation material can be summarized in a single material performance index $M = (\lambda \cdot C_p \cdot \rho)^{1/2}$ by which different thermal insulation can be ranked in terms of performances as building thermal insulator panels. Normally, heating and cooling loads are not constant during the day but are tailored to maintain internal comfort during residency. In hot and warm climates, especially those with large diurnal temperature variation (e.g. southern Europe), a high heat capacity is preferred since it helps to stabilize the internal temperature due to the thermal damping effect. Converseley, in cold climates (e.g. northern Europe), with an extensive use of internal heating, a wall with a high thermal capacity can have a detrimental effect since more heat is lost through the wall heating (Carlos, 2017; Reilly & Kinnane, 2017).

On those grounds, materials with a lower M index perform well in cold climate whereas in hot – warm climate materials performance follows the highest value of M (see Appendix A in Supporting information for detailed calculation). In Fig. 8 several thermal insulation

Table 2
Density and thermal properties of oAF, rAF and 2rAF. Mean absolute deviation in parentheses.

Sample	Density [kg/m^3]	Thermal Conductivity 20 °C [mW/ m K]	Thermal Conductivity 40 °C [mW/ m K]	Specific heat capacity 20 °C [KJ/m^3 k]	Specific heat capacity 30 °C [KJ/m^3 k]
oAF	78.26 (7.19)	43.23 (0.22)	48.64 (0.70)	1.11 (0.07)	1.19 (0.09)
rAF – G	127.91 (6.96)	49.23 (0.86)	59.06 (0.33)	1.57 (0.02)	1.75 (0.02)
rAF – GC	120.57 (5.45)	47.80 (1.20)	54.18 (1.35)	1.49 (0.02)	1.74 (0.01)
rAF – G – A	128.95 (2.26)	47.77 (0.46)	56.18 (3.49)	1.46 (0.06)	1.75 (0.04)
rAF – GC – A	137.19 (2.61)	44.80 (0.24)	49.63 (1.45)	1.31 (0.06)	1.51 (0.13)
2 rAF – G	157.19	53.73	68.52	1.93	1.99

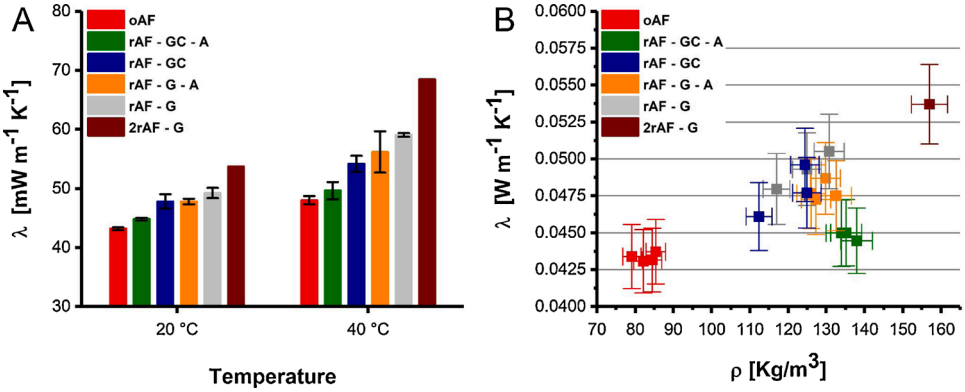

Fig. 6. Thermal conductivity of oAF, rAF and 2rAF composites. (A) average thermal conductivity values are presented, with the corresponding average absolute error. (B) a plot of density vs thermal conductivity at 20 °C of each tested specimen. A relative instrumental precision error of 5 % and 3 % was attributed to each single measurement, respectively for thermal conductivity and density.

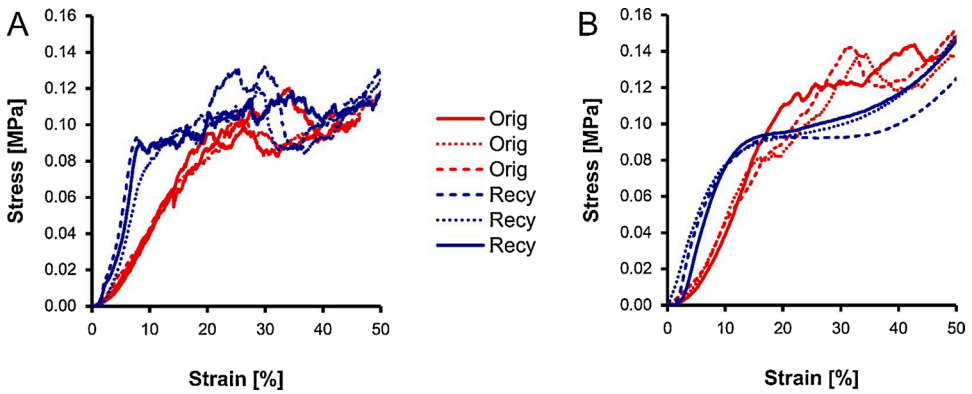

Fig. 7. Compression resistance of oAF (Orig) and rAF – G (recy) tested as-lyophilized (A) and conditioned at 40 RH (B).

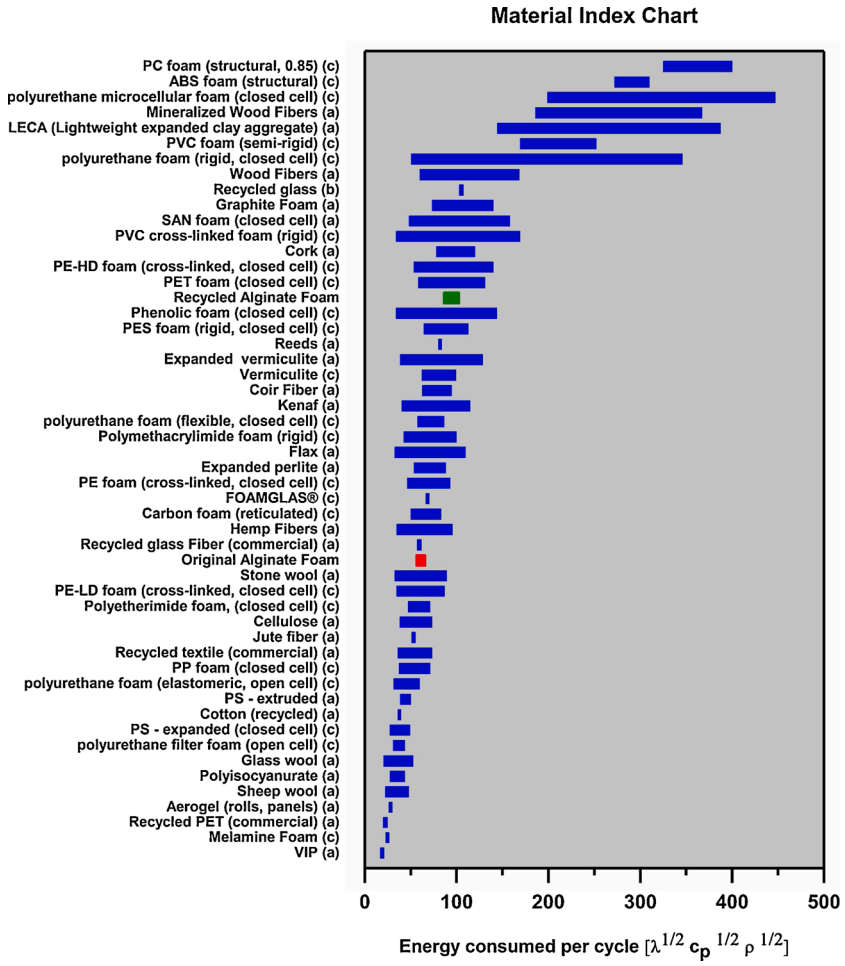

Fig. 8. Thermal insulation material performance sorted by material index M. Data source: a) (Schiavoni, D'Alessandro, Bianchi, & Asdrubali, 2016) b) (Asdrubali et al., 2015) c) CES Selector 2018. Data for the original and the recycled alginate foam (grouped), respectively in red and green, from Table 2.

materials are sorted by M and it can be seen that the rAF remains competitive against commercial options and natural alternatives. In Fig. 6 are also presented the thermal properties of 2 r – AF; the same considerations stated above for r – AF about the increased density and thermal conductivity apply. The problem related to the increased density can be easily addressed by addition of new alginate (to increase the matrix volume) and is not associated to the chelation-driven recycling process herein described – which, instead, has been proved to be effective in a second recycling test. The presence of the chelator in the r – AF, in an inactive form, confers an added value to the new recycled material which can be therein recycled multiple times without addition of a new chelating agent.

4.5. *Mechanical properties*

Fig. 7 reports a typical compression stress-strain curve of an oAF and a rAF – G tested as-lyophilized (Fig. 7A) and after a conditioning treatment at 40 RH (Fig. 7B). No statistically significant differences were detected in the mechanical properties between any of the rAF and oAF samples tested in the "as-lyophilized" condition.

Both the original and the recycled material showed a brittle behavior, with a failure stress at around 80–200 kPa. Interestingly, after conditioning in a 40RH chamber, a marked visco-elastic behavior emerges in all rAF samples. This is probably caused by the higher GDL content in rAF samples.

Weight gain due to water uptake stops (on average) at 0.8 % and 3 % for oAF and rAF samples, respectively. 40 h-conditioned rAF samples were capable to recover 75 % of the compression strain, compared to the 30 % of the oAF (after a compression strain of 50 %). Compressive Strain and Young's Modulus data are detailed in Supporting information Table S6

5. Conclusion

We have demonstrated a simple recycling process which, by using a chelating agent easily controlled via pH, is capable to dismantle and rebuild the matrix of an ionotropic alginate-based composite. The functionality of the original material is fully maintained.

As a proof of concept, we recycled an alginate foam, which was previously developed as thermal and sound insulation system. The field of application of this process is not limited to alginate-based systems but can in principle be applied to recycle any composite material, the matrix of which is stabilized by ion-polymer junctions. This includes other polyanionic systems such as: hyaluronic acid, pectin and cellulose.

In the specific case examined here, we were able to fully recycle the original material maintaining or improving its thermal, sound and mechanical properties.

Morphology and thermal characterization highlighted that control of the porous structure could lead to major performance improvement. This could be easily done by adopting different freezing techniques (e.g. liquid nitrogen deep freezing) regardless of the original adopted technique, shape, dimension, density and microstructure of the oAF, since these characteristics are lost in the process. In a similar fashion, the properties of the recycled material can be tailored to new specific target applications: flame retardants, anti-fungal chemicals and plasticizer can be easily added after the alginate matrix dissolution.

As clearly stated previously, the selection of the best thermal insulation option does not rely only on thermal properties but also strongly depends on local variables (e.g. climate, place of installation and occupancy profile of the building). Based on these assumptions the recycled material, as presented in this work, represents a valid alternative to commercial options.

The process demonstrated here lends itself to a cradle-to-cradle approach: due to the presence of the chelating agent in the recycled material, multiple recycling cycles can be performed, simply by activating it in a basic aqueous environment. Additionally, the recycling process, within the herein described specific application, has proved to be robust with respect to the process parameters which is, together with the unnecessarily needs of specialized equipment, an undoubtedly valuable advantage in terms of industrial scalability.

CRediT authorship contribution statement

Matteo Cibinel: Conceptualization, Methodology, Investigation, Formal analysis, Writing - original draft. **Giorgia Pugliese:** Investigation, Formal analysis. **Davide Porrelli:** Investigation, Formal analysis. **Lucia Marsich:** Writing - review & editing. **Vanni Lughi:** Supervision, Funding acquisition, Writing - review & editing.

Acknowledgements

The authors would like to thank prof. Romani Lapasin for his help provided during rheological data evaluation.

This work was supported by "GGTDoors – Green Gas Tight Doors" project funded by Regione Autonoma Friuli Venezia Giulia, POR-FESR 2014-2020.

Appendix A. Supplementary data

Supplementary material related to this article can be found, in the online version, at doi:https://doi.org/10.1016/j.carbpol.2020.116995.

References

Agulhon, P., Robitzer, M., David, L., & Quignard, F. F. (2012). Structural regime identification in ionotropic alginate gels: Influence of the cation nature and alginate structure. *Biomacromolecules, 13*(1), 215–220.

Ardente, F., Beccali, M., Cellura, M., & Mistretta, M. (2008). Building energy performance: A LCA case study of kenaf-fibres insulation board. *Energy and Buildings, 40*(1), 1–10.

Asdrubali, F., D'Alessandro, F., & Schiavoni, S. (2015). A review of unconventional sustainable building insulation materials. *Sustainable Materials and Technologies, 4* (2015), 1–17.

Asdrubali, F., Schiavoni, S., & Horoshenkov, K. V. (2012). A review of sustainable materials for acoustic applications. *Building Acoustics, 19*(4), 283–312.

Ayadi, A., Stiti, N., Boumchedda, K., Rennai, H., & Lerari, Y. (2011). Elaboration and characterization of porous granules based on waste glass. *Powder Technology, 208*(2), 423–426.

Bassett, D. C., Håti, A. G., Melø, T. B., Stokke, B. T., & Sikorski, P. (2016). Competitive ligand exchange of crosslinking ions for ionotropic hydrogel formation. *Journal of Materials Chemistry B, 4*(37), 6175–6182.

Brun, F., Mancini, L., Kasae, P., Favretto, S., Dreossi, D., & Tromba, G. (2010). Pore3D: A software library for quantitative analysis of porous media. *Nuclear Instruments and Methods in Physics Research, Section A: Accelerators, Spectrometers, Detectors and Associated Equipment, 615*(3), 326–332.

Caniato, M., & Travan, A. (2016). EP Patent 16425023.5.

Caniato, M., Sbaizero, O., Schmid, C., & Bettarello, F. (2015). Recycled materials for noise reduction in floating floors. In *22nd International Congress on Sound and Vibration, ICSV 2015. International Institute of Acoustics and Vibrations*.

Cao, L., Fu, Q., Si, Y., Ding, B., & Yu, J. (2018). Porous materials for sound absorption. *Composites Communications, 10*(June), 25–35.

Carlos, J. S. (2017). The impact of thermal mass on cold and hot climate zones of Portugal. *Indoor and Built Environment, 26*(6), 733–743.

Cross, M. M. (1969). Polymer rheology: Influence of molecular weight and polydispersity. *Journal of Applied Polymer Science, 13*(4), 765–774.

Erkmen, J., Yavuz, H. I., Kavci, E., & Sari, M. (2020). A new environmentally friendly insulating material designed from natural materials. *Construction and Building Materials, 255*, Article 119357.

Guarino, V., Caputo, T., Altobelli, R., & Ambrosio, L. (2015). Degradation properties and metabolic activity of alginate and chitosan polyelectrolytes for drug delivery and tissue engineering applications. *AIMS Materials Science, 2*(4), 497–502.

Harrison, P., Holmes, P., Bevan, R., Kamps, K., Levy, L., & Greim, H. (2015). Regulatory risk assessment approaches for synthetic mineral fibres. *Regulatory Toxicology and Pharmacology, 73*(1), 425–441.

Haug, A., Larsen, B., Smidsröd, O., Munch-Petersen, J., & Munch-Petersen, J. (1963). The degradation of alginates at different pH values. *Acta Chemica Scandinavica, 17*, 1466–1468.

Ivanova, E. P., Bazaka, K., & Crawford, R. J. (2014). Natural polymer biomaterials: Advanced applications. In E. P. Ivanova, K. Bazaka, & R. J. Crawford (Eds.), *New functional biomaterials for medicine and healthcare* (pp. 32–70). Elsevier.

Kemona, A., & Piotrowska, M. (2020). Polyurethane recycling and disposal: Methods and prospects. *Polymers, 12*(8), 1752.

Kyaw Oo D'Amore, G., Travan, A., Marsich, L., Ferluga, A., Caniato, M., Schmid, C., … Turco, G. (2017). Innovative thermal and acoustic insulation foam from recycled waste glass powder. *Journal of Cleaner Production, 165*, 1306–1315.

Lacoste, C., El Hage, R., Bergeret, A., Corn, S., & Lacroix, P. (2018). Sodium alginate adhesives as binders in wood fibers/textile waste fibers biocomposites for building insulation. *Carbohydrate Polymers, 184*, 1–8.

Lassen, C., Warming, M., Jakobsen, L. G., Novichkov, B., Strand, J., Feld, L., … Bach, L. (2019). *Survey of polystyrene foam (EPS and XPS) in the Baltic Sea* (February).

Lee, K. Y., & Mooney, D. J. (2012). Alginate: Properties and biomedical applications. *Progress in Polymer Science, 37*(1), 106–126.

Masson-Delmotte, V., Zhai, H. O. P., Roberts, D., Skea, J., P. R. S., Pirani, A., Moufouma-Okia, W., … Waterfield, T. (2018). *Global warming of 1.5°C. An IPCC Special Report on the impacts of global warming of 1.5°C above pre-industrial levels and related global greenhouse gas emission pathways, in the context of strengthening the global response to the threat of climate change*.

Mati-Baouche, N., De Baynast, H., Lebert, A., Sun, S., Lopez-Mingo, C. J. S., Leclaire, P., … Michaud, P. (2014). Mechanical, thermal and acoustical characterizations of an insulating bio-based composite made from sunflower stalks particles and chitosan. *Industrial Crops and Products, 58*, 244–250.

Muthuraj, R., Lacoste, C., Lacroix, P., & Bergeret, A. (2019). Sustainable thermal insulation biocomposites from rice husk, wheat husk, wood fibers and textile waste fibers: Elaboration and performances evaluation. *Industrial Crops and Products, 135* (May), 238–245.

Nguyen, S. T., Tran-Le, A. D., Vu, M. N., To, Q. D., Douzane, O., & Langlet, T. (2016). Modeling thermal conductivity of hemp insulation material: A multi-scale homogenization approach. *Building and Environment, 107*, 127–134.

Palumbo, M., Lacasta, A. M., Navarro, A., Giraldo, M. P., & Lesar, B. (2017). Improvement of fire reaction and mould growth resistance of a new bio-based thermal insulation material. *Construction and Building Materials, 139*, 531–539.

Palumbo, M., Navarro, A., Giraldo, P., Lesar, B., & Lacasta, A. M. (2015). Performance of biobased insulation board from crop byproducts and natural gums. *Academic Journal of Civil Engineering, 33*(2), 189–196.

Pavel, C. C., & Blagoeva, D. T. (2018). *Competitive landscape of the EU's insulation materials industry for energy-efficient buildings, EUR 28816 EN*. Luxembourg: Publications Office of the European Union, 2018, PUBSY No. JRC10869.

Qin, Y., Jiang, J., Zhao, L., Zhang, J., & Wang, F. (2018). Applications of alginate as a functional food ingredient. In A. M. Grumezescu, & A. M. Holban (Eds.), *Biopolymers for food design* (pp. 409–429). Elsevier.

Reilly, A., & Kinnane, O. (2017). The impact of thermal mass on building energy consumption. *Applied Energy, 198*(April 2017), 108–121.

Roopa, B. S., & Bhattacharya, S. (2009). Characterisation and modelling of time-independent and time-dependent flow behaviour of sodium alginate dispersions. *International Journal of Food Science & Technology, 44*(12), 2583–2589.

Schiavoni, S., D'Alessandro, F., Bianchi, F., & Asdrubali, F. (2016). Insulation materials for the building sector: A review and comparative analysis. *Renewable and Sustainable Energy Reviews, 62*, 988–1011.

Sergeeva, A., Vikulina, A. S., & Volodkin, D. (2019). Porous alginate scaffolds assembled using vaterite CaCO3 crystals. *Micromachines, 10*(6), 357.

Thakur, S., Verma, A., Sharma, B., Chaudhary, J., Tamulevicius, S., & Thakur, V. K. (2018). Recent developments in recycling of polystyrene based plastics. *Current Opinion in Green and Sustainable Chemistry, 13*, 32–38.

Ürge-Vorsatz, D., Cabeza, L. F., Serrano, S., Barreneche, C., & Petrichenko, K. (2015). Heating and cooling energy trends and drivers in buildings. January 1 *Renewable and Sustainable Energy Reviews*. Elsevier Ltd..

Valverde, I. C., Castilla, L. H., Nuñez, D. F., Rodriguez-Senín, E., & De La Mano Ferreira, R. (2013). Development of new insulation panels based on textile recycled fibers. *Waste and Biomass Valorization, 4*(1), 139–146.

Vincent, T., Dumazert, L., Dufourg, L., Cucherat, C., Sonnier, R., & Guibal, E. (2018). New alginate foams: Box-Behnken design of their manufacturing; fire retardant and thermal insulating properties. *Journal of Applied Polymer Science, 135*(7), 1–12.

Yamamoto, K., Yuguchi, Y., Stokke, B. T., Sikorski, P., & Bassett, D. C. (2019). Local structure of Ca2+ alginate hydrogels gelled via competitive ligand exchange and measured by small angle X-ray scattering. *Gels, 5*(1).

Zheng, H., Gao, M., Ren, Y., Lou, R., Xie, H., Yu, W., … Ma, X. (2017). An improved pH-responsive carrier based on EDTA-Ca-alginate for oral delivery of Lactobacillus rhamnosus ATCC 53103. *Carbohydrate Polymers, 155*, 329–335.